analytical chemistry

Article

pubs.acs.org/ac

Dynamic Evaluation of Cell Surface *N*-Glycan Expression via an Electrogenerated Chemiluminescence Biosensor Based on Concanavalin A-Integrating Gold-Nanoparticle-Modified $Ru(bpy)_3^{2+}$-Doped Silica Nanoprobe

Zhuhai Chen, Yang Liu, Yangzhong Wang, Xin Zhao, and Jinghong Li*

Department of Chemistry, Beijing Key Laboratory for Analytical Methods and Instrumentation, Tsinghua University, Beijing 100084, China

Supporting Information

ABSTRACT: A sandwich electrogenerated chemiluminescence (ECL) biosensor was fabricated based on concanavalin A (Con A)-integrating gold-nanoparticle-modified $Ru(bpy)_3^{2+}$-doped silica nanoprobe (Au−$RuSiO_2$ NPs) for in situ and dynamically evaluating cell surface *N*-glycan expression. Owing to the specific recognition of Con A with mannose and the core trimannoside fragment of *N*-glycan and the effective ECL amplification of Au−$RuSiO_2$ NPs, the as-proposed biosensor exhibited excellent analytical performance toward the cytosensing of K562 cells with a wide detection linear range from 1.0×10^3 to 1.0×10^7 cells mL^{-1} and a detection limit of 600 cells mL^{-1}. More importantly, the strategy was successfully applied to evaluate cell surface *N*-glycan expression under different external stimuli of inhibitors and enzyme. This biosensor is endowed with feasibility and reliability of generating sensitive insight into the majority of *N*-glycan expression on the cell surface. Furthermore, the biosensor was employed to dynamically profile cell surface *N*-glycan expression at different phases of cell growth in vitro. This biosensor is promising in studying and elucidating the *N*-glycan function in biological and physiological processes.

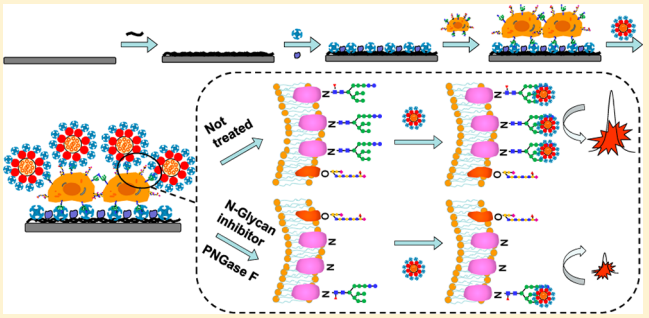

Carbohydrates are found to be covalently attached to underlying proteins or lipids with high density and complex diversity on the exterior surface of all the cells of every eukaryotic species.[1,2] It is not surprising that carbohydrates on the cell surface play vital roles in a broad range of crucial biological and physiological processes, including growth, development, differentiation, cell adhesion, cell−cell communication, signaling, immune response, disease, and progression of cancer.[2−7] Among various carbohydrates, mannose is one of the 10 monosaccharides that are the building blocks of all the mammalian glycans with diverse sequences and structures.[8] Mannose with its binding proteins or receptors mediates a large number of biological events. For example, the binding between the terminal high-mannose type oligosaccharide and the mannose receptor on the cell surface is involved in the process of cellular fusion in osteoclast formation.[9] In addition, mannose is the core fragment of *N*-glycans on the cell surface that share a common pentasaccharide core structure consisting of Manα1−6(Manα1−3)Manβ1−4GlcNAcβ1−4GlcNAc despite the terminal sugars with diverse and complex structures.[2,10,11] The variational expression of cell surface mannose within *N*-glycan is observed in the course of tumorigenesis, brain aging, and differentiation.[12] Therefore, it is significant to evaluate cell surface mannose and *N*-glycan expression for deciphering their roles in biological processes and clinical analysis.

To date, a series of approaches have been developed for glycan analysis, including high-performance liquid chromatography (HPLC),[13] mass spectrometry (MS),[14−16] nuclear magnetic resonance (NMR),[17] and capillary electrophoresis (CE)[18] involving chemical label or chemical and/or enzymatic release of the carbohydrates, either alone or in combination. Although these well-established methods are powerful for revealing structural details, they are time-consuming, with complicated sample preparation and sophisticated instrumentation, and not feasible for profiling surface glycans of living cells due to their destructive procedures. Recently, glyco-biosensors such as lectin arrays[19] and electrochemical biosensors[20−22] based on lectins, a group of carbohydrate-specific binding proteins,[23] have been greatly developed to complement the limitation with potential ability for simple and rapid analysis of carbohydrates.[24]

Electrogenerated chemiluminescence (ECL), a powerful analytical technique combining electrochemical and lumines-

Received: December 25, 2012
Accepted: April 8, 2013
Published: April 8, 2013

   dx.doi.org/10.1021/ac303572g | *Anal. Chem.* 2013, 85, 4431−4438

Scheme 1. Schematic Illustration of ECL Biosensor for Dynamic Evaluation of Cell Surface *N*-Glycan Expression Based on Con A: (A) Fabrication Procedures of Con A@Au−$RuSiO_2$ NPs and (B) ECL Biosensor for Cytosensing and Evaluating Cell Surface *N*-Glycan Expression Based on Con A@Au−$RuSiO_2$ NPs

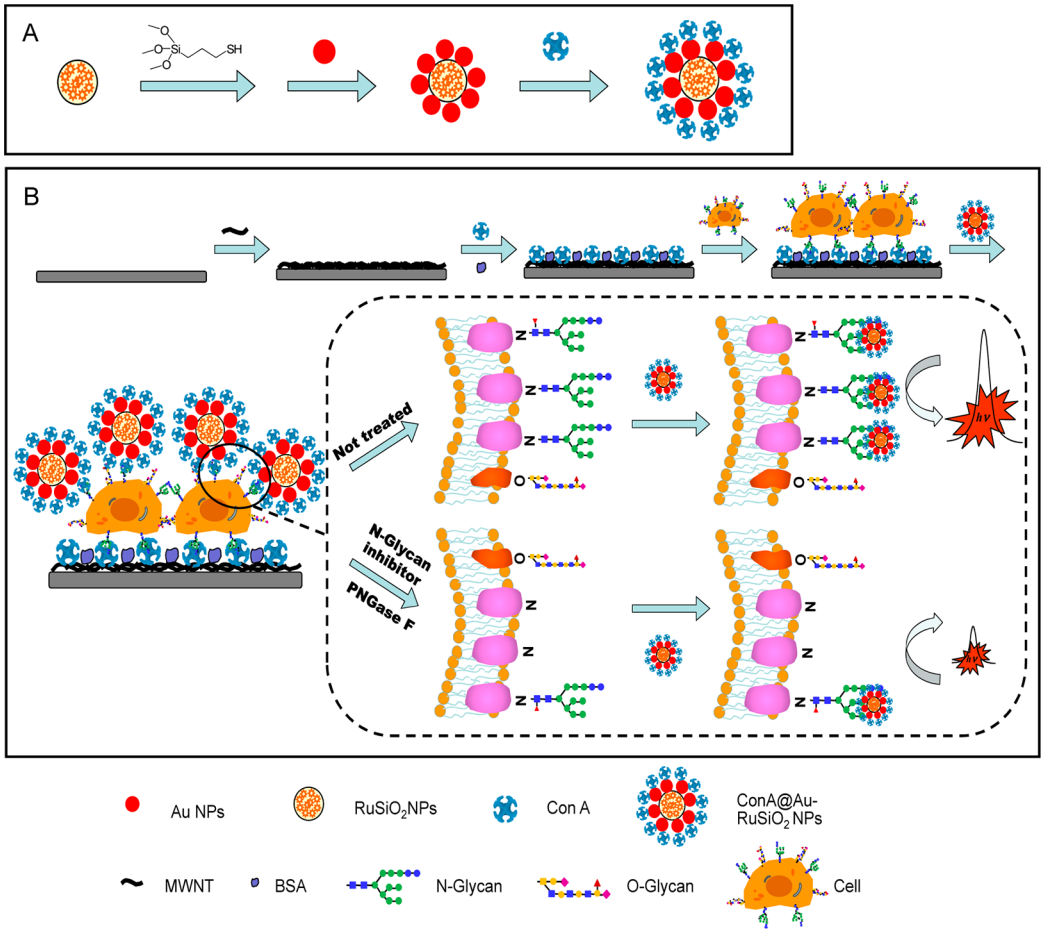

cent methods, has attracted considerable interest for its distinct advantages, such as low cost, low background noise, high sensitivity, and potential and spatial controllability.[25] ECL biosensor has been widely used in immunoassay,[26] DNA analysis,[27] and clinical diagnosis.[28] With excellent optical, electrical, and electrochemical properties, the nanoparticles can work as promoters to afford substantial ECL signal amplification and enhance the performance of the biosensors.[26] Silica nanoparticles have been demonstrated to be a good matrix for immobilizing a high concentration of $Ru(bpy)_3^{2+}$ to promote ECL detection with ease of modification and functionalization on the surface.[29] At the same time, owing to their unique properties, such as good biocompatibility, fascinating electrocatalytic activity, excellent conductivity, and large surface area, gold nanoparticles (Au NPs) have been extensively used in ECL biosensors.[27,29,30] Au NPs can also be used as carriers of proteins like enzyme and antibody to construct biosensors.[31,32]

Concanavalin A (Con A), from *Canavalia ensiformis*, specifically recognizes and binds to mannose, and it has a much higher affinity to oligomannose, especially the trimannoside Manα1−6(Manα1−3)Man, which is the core oligosaccharide segment of *N*-glycan.[33−36] Glycoproteins on cell surface containing high mannose, hybrid, and biantennary complex types of *N*-glycan can be bound by Con A.[37] In this case, Bunkenborg et al.[38] and Koles et al.[39] used Con A to catch and enrich N-linked glycoproteins for further mapping the N-glycosylated sites of glycoproteins. Thus, most *N*-glycans on the cell surface could be recognized and monitored by Con A through the affinity of the trimannoside motif.

In this work, a sandwich biosensor based on Con A was designed and implemented by integrating gold-nanoparticle-modified $Ru(bpy)_3^{2+}$-doped silica nanoprobe for dynamic profiling of cell surface mannose and *N*-glycan expression. Con A, as the recognizer and capturer for cells via the specific affinity to mannose and the core trimannoside of *N*-glycan on the cell surface, was used to form the sandwich architecture (Scheme 1). The utilization of twice the Con A for capture of cell and attachment of ECL nanoprobe could enhance the selectivity of the biosensor for sensing glycans on the cell surface. Besides, the assembled Au NPs on nanoprobes could increase the surface area for immobilizing much Con A and improve the electron transfer for enhancing ECL signal of the $Ru(bpy)_3^{2+}$-doped SiO_2 nanoparticles ($RuSiO_2$ NPs). When Con A-based gold-nanoparticle-modified $Ru(bpy)_3^{2+}$-doped silica composite nanoprobes (Con A@Au−$RuSiO_2$ NPs) bind to the cell surface, the expression of mannose and most *N*-glycans could be evaluated through the amplified ECL signal of $Ru(bpy)_3^{2+}$. The proposed Con A-based ECL biosensor could significantly respond to the change of cell surface carbohydrates disturbed by the external stimuli of *N*-glycan inhibitor tunicamycin (TM) or released by peptide-*N*-glycosidase F

dx.doi.org/10.1021/ac303572g | *Anal. Chem.* 2013, 85, 4431−4438

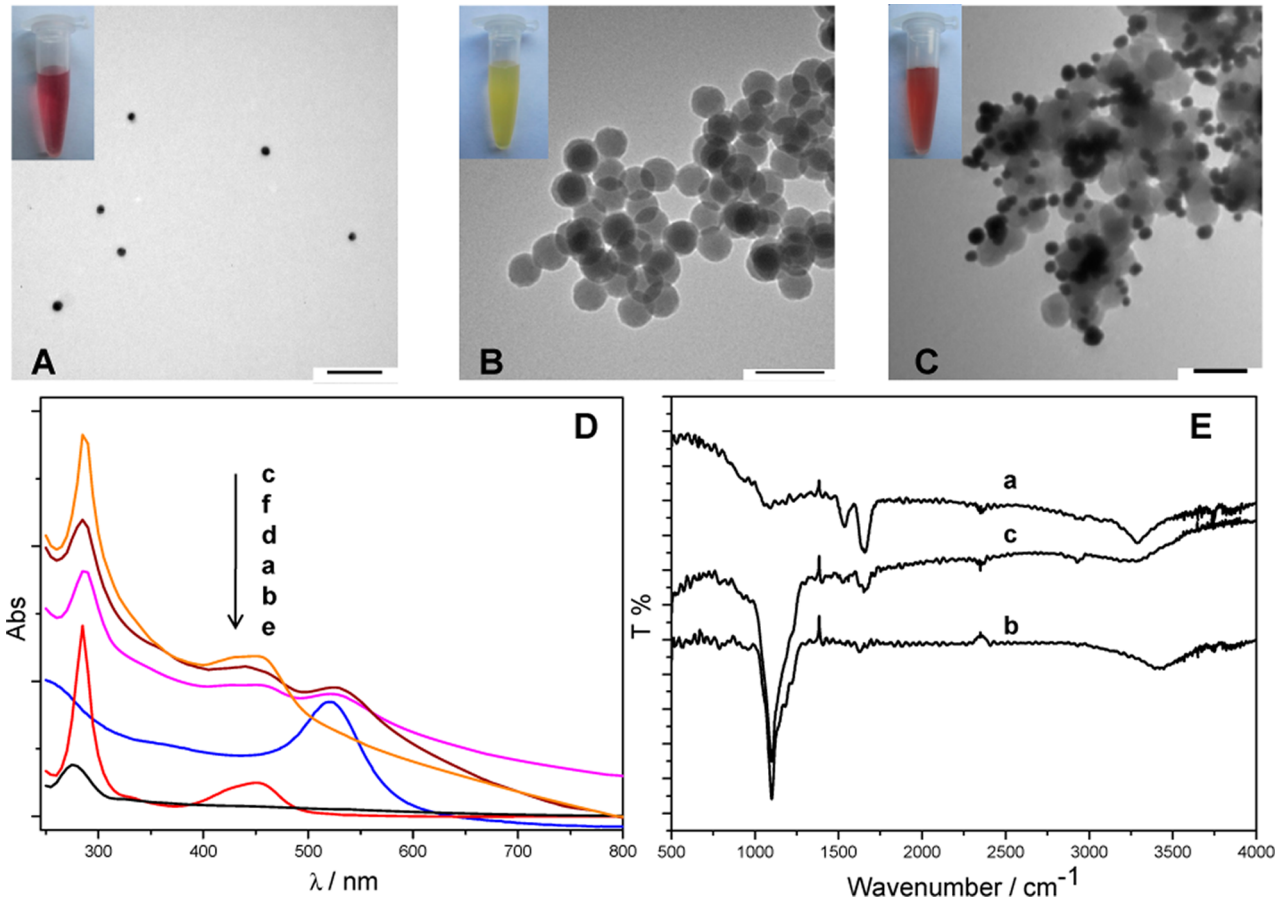

Figure 1. TEM images of Au NPs (A), $RuSiO_2$ NPs (B), and Au−$RuSiO_2$ NPs (C). Inset: Photographs of Au NPs (A), $RuSiO_2$ NPs (B), and Au−$RuSiO_2$ NPs (C). Scale bar: 100 nm. (D) UV−vis spectra of Au NPs (a, blue), $Ru(bpy)_3^{2+}$ (b, red), $RuSiO_2$ NPs (c, orange), Au−$RuSiO_2$ NPs (d, magenta), Con A (e, black), and Con A@Au−$RuSiO_2$ NPs (f, wine). (E) FTIR spectra of Con A (a), Au−$RuSiO_2$ NPs (b), and Con A@Au−$RuSiO_2$ NPs (c).

(PNGase F), while as compared to untreated cells, slight signal change was observed by the *O*-glycan inhibitor benzyl 2-acetamido-2-deoxy-α-D-galactopyranoside (BG). Thus, these results prove the feasibility and reliability of analyzing cell surface *N*-glycan expression via the proposed glyco-biosensor. Then, the as-proposed biosensor was applied to monitor in situ cell surface *N*-glycan expression at different phases of cell growth in vitro. This sensitive biosensor could provide an important tool to evaluate the *N*-glycan expression on the cell surface and open a new way to understand the physiological functions of glycans in the cellular processes as well as clinical analysis of glycoprotein related diseases.

EXPERIMENTAL SECTION

Reagents and Materials. Con A, fluorescein isothiocyanate conjugated Concanavalin A (FITC−Con A), and TM were purchased from Sigma-Aldrich. Tri-*n*-propylamine (TPA), 1-(3-Dimethylaminopropyl)-3-ethylcarbodiimide hydrochloride (EDC), and *N*-hydroxysulfosuccinimide sodium salt (NHSS) were obtained from Alfa Aesar. BG was gotten from Toronto Research Chemical Inc. (Canada). PNGase F was obtained from New England Biolabs Inc. (Ipswich, MA). Bovine serum albumin (BSA) was from Dingguo Biological Products Co. (Beijing, China). Other regents of analytical grade were obtained from Beijing Chemical Co. (Beijing, China).

Cell Culture and Cell Treatment. The K562 cell line was kindly provided by the Medicine School of Tsinghua University, Beijing, China. K562 cells were cultured in RPMI 1640 medium (Dingguo Biological Products Co., Beijing, China) supplemented with 10% fetal calf serum (Zhejiang Tianhang Biological Technology Co., Ltd., Zhejiang, China), 100 U mL^{-1} penicillin, and 100 μg mL^{-1} streptomycin at 37 °C in a humidified atmosphere of 5% CO_2. The cells were grown to midlog phase and then collected and separated from the medium by centrifugation at 1000 rpm for 5 min and then washed with sterile phosphate buffer saline (PBS, pH 7.4) twice. The sediment was resuspended in sterile PBS containing 1 mM Ca^{2+} and Mn^{2+} to obtain a homogeneous cell suspension. Here, the divalent cations Ca^{2+} and Mn^{2+} were required for the activity of Con A binding to cell surface mannose.

For evaluating the inhibition effect of the cell surface carbohydrate expression under external stimulation of TM and BG, K562 cells were seeded to culture plate at the density of 2 × 10^5 cells mL^{-1} and then incubated in the culture medium respectively containing 1 μg mL^{-1} (approximate 1.2 μM) TM and 500 μM BG for 0−48 h. Enzymatic cleavage of the *N*-glycans from cell surface was conducted using PNGase F, and 2000 NEB units of PNGase F was added to the cell suspension with concentration of 5 × 10^5 cells mL^{-1} containing 2% BSA and then mildly shaken for 24 h. Besides, the cells primarily inhibited by 1 μg mL^{-1} TM or 500 μM BG for 48 h were also chosen for enzymatic digestion following the same procure above. Cells at different phases of cell growth were obtained

dx.doi.org/10.1021/ac303572g | Anal. Chem. 2013, 85, 4431−4438

after cells were seeded to culture plate at the density of 2×10^5 cells mL^{-1} without passaging for 7 days of continuous culture.

Biosensor Preparation and Cell Capture. A glassy carbon electrode (GCE, diameter of 3 mm) was successively polished with 0.3 and 0.05 μm α-Al_2O_3 slurry on an abrasive cloth and thoroughly cleaned with ethanol and distilled water under ultrasonication. After being dried with high-purity nitrogen gas, 6 μL of 0.25 mg mL^{-1} carboxylic group functionalized multiwall carbon nanotubes (MWNT) solution was first dropped onto the pretreated GCE and dried overnight at room temperature to yield the MWNT-modified GCE (MWNT/GCE). Then, the electrode was immersed in 50 μL of a mixture aqueous solution containing 100 mM EDC and 250 mM NHSS at 37 °C for 3.5 h. The immobilization of Con A was accomplished by incubating the MWNT/GCE electrode into 50 μL of 2 mg mL^{-1} Con A solution at 37 °C for 2 h. Whereafter, the washed electrode was immersed in 2 mg mL^{-1} BSA for 30 min at 37 °C to block the excess active groups on the surface. Thus, Con A-modified electrode GCE/MWNT/Con A was prepared following a thorough rinse with PBS and used for cell capture. After that, the electrode was soaked in 100 μL of K562 cell suspension at a certain concentration and incubated at 37 °C for 80 min to capture the cells via the specific binding between Con A and cell surface mannose and trimannoside. Subsequently, the obtained Cell/Con A/MWNT/GCE electrode was taken out, carefully rinsed with PBS to remove the noncaptured cells, and used for subsequent ECL characterization assays.

ECL Characterization of Nanoprobe-Based Cell Surface *N*-Glycan Expression. The Cell/Con A/MWNT/GCE electrode was incubated with 10 μL of the ECL nanoprobe Con A@Au−$RuSiO_2$ NPs solution for 60 min at 37 °C. Finally, the electrode was washed carefully and thoroughly with PBS to remove nonspecifically bound nanoprobes to minimize the background response. The resulting electrode was characterized via ECL measurement in a 0.1 M PBS solution (pH 7.4) with 5 mM TPA using Ag/AgCl electrode with saturated KCl solution and platinum wire as the reference electrode and counter electrode, respectively. The ECL measurements were performed from 0.2 to 1.25 V with scan rate of 100 mV s^{-1}.

RESULTS AND DISCUSSION

Nanoprobe-Based ECL Strategy for Cytosensing and Evaluating Cell Surface *N*-Glycan Expression. The ECL strategy for cytosensing and evaluating cell surface *N*-glycan expression based on Con A is illustrated in Scheme 1. MWNT was first coated onto the surface of GCE in order to increase the electron transfer rate between electrode interface and electroactive substance. The resulting MWNT film also provided plenty of sites for the immobilization of Con A due to its high specific surface area. Adequate Con A on the electrode further ensured the efficiency of the following cell capture by the specific interaction of Con A with mannose or trimannoside, the core oligosaccharide of *N*-glycan on cell surface. After cells were captured, the electrode was incubated with the previously prepared ECL nanoprobe of Con A@Au−$RuSiO_2$ NPs to form a sandwich type system, where implementation of attachment was still based on the binding affinity between Con A and mannose. The designed biosensor employs a sandwich system using twice the Con A for capture of cell and attachment of ECL nanoprobe, achieving higher selectivity of cell surface glycan. Meanwhile, Con A@Au−$RuSiO_2$ NPs exploit the amplification effect of Au NPs for loading a large number of Con A and enhancing the ECL activity of $Ru(bpy)_3^{2+}$-doped SiO_2 nanoparticles ($RuSiO_2$ NPs).[40] Thus, the sensitivity of the biosensor is greatly enhanced for cytosensing and analysis of cell surface *N*-glycan expression.

Characterization of the Nanoprobe. As shown in Figure 1A, the citrate reduced Au NPs were well-dispersed particles with diameter of ∼15 nm. The color of Au NPs colloid was wine red (inset of Figure 1A). The TEM image of the prepared $RuSiO_2$ NPs is displayed in Figure 1B. $RuSiO_2$ NPs with the diameter of ∼55 nm were much larger than Au NPs, so one $RuSiO_2$ NP could load several Au NPs to form Au−$RuSiO_2$ NPs. The as prepared Au−$RuSiO_2$ NPs are showed in Figure 1C.

Figure 1D shows the UV−vis absorption spectra of Au NPs, $Ru(bpy)_3^{2+}$, $RuSiO_2$ NPs, Au−$RuSiO_2$ NPs, Con A, and Con A@Au−$RuSiO_2$ NPs, respectively. Obviously, for Au NPs colloid, the absorbance peak appeared at 520 nm. $Ru(bpy)_3^{2+}$ exhibited two characteristic peaks at 285 and 450 nm, which are assigned to ligand-centered ($\pi \rightarrow \pi^*$) transitions and metal-to-ligand charge transfer adsorption, respectively.[41,42] The synthesized $RuSiO_2$ NPs had two similar peaks, suggesting that more molecules $Ru(bpy)_3^{2+}$ were doped into SiO_2 NPs successfully through the electrostatic interaction between $Ru(bpy)_3^{2+}$ and silica nanoparticles. After that, Au NPs were assembled onto the $RuSiO_2$ NPs surfaces via the strong interaction between Au NPs and −SH groups. The spectrum of Au−$RuSiO_2$ NPs shows the characteristic absorption peak of Au NPs, indicating the effective assembly. When Con A was conjugated to the Au−$RuSiO_2$ NPs, a 285 nm absorption peak with a little wider width and a slight shoulder at 275 nm was observed besides the two visible absorption peaks. The absorption band of 275 nm is assigned to the protein Con A (curve e in Figure 1D). These results indicate that the fabrication of the ECL nanoprobe Con A@Au−$RuSiO_2$ NPs was achieved.

Additionally, successful conjugation was also confirmed by the FTIR spectroscopy shown in Figure 1E. Apparently, after Con A coupling, two new absorption bands corresponding to amide bands I (C═O stretching) and II (N−H bending) located at 1657 and 1531 cm^{-1}, respectively, which were consistent with pure Con A, were seen. The strong peak at 1100 cm^{-1} ascribed to the Si−O−Si stretching vibration[42,43] was seen in both Au−$RuSiO_2$ NPs and Con A@Au−$RuSiO_2$ NPs. Thus, these results demonstrate the successful synthesis of the ECL nanoprobe Con A@Au−$RuSiO_2$ NPs.

Electrochemical Characterizations of the Biosensor. Cyclic voltammetry (CV) and electrochemical impedance spectroscopy (EIS) are powerful and facile electrochemical techniques to verify the assembly processes of the modified electrodes step by step. Figure S1A (Supporting Information) displays the CV curves to characterize the fabrication procedures of the modified GCE using $Fe(CN)_6^{4-/3-}$ as electroactive probes. The bare GCE exhibited a couple of reversible redox peaks in curve a. After the electrode was modified with MWNT, the peak currents of the electrode increased (curve b). The increasing response is attributed to the large surface and the excellent electrical conductivity of MWNT. When Con A was immobilized onto the above electrode, an obvious decrease in the amperometric signal was found (curve c). The peak currents in the CV were further decreased, and the gap between the anodic and cathodic peaks became wider after subsequent capture of K562 cells by the

dx.doi.org/10.1021/ac303572g | Anal. Chem. 2013, 85, 4431−4438

specific binding between Con A and the cell surface mannose (curve d). The phenomenon resulted from the electron inert feature of Con A and cells that blocks the electron transfer and mass transfer of $Fe(CN)_6^{4-/3-}$ ions at the modified GCE surface. Finally, the biosensor is incubated with the Con A@Au−$RuSiO_2$ NPs. The whole nanoprobe is negatively charged due to the negatively charged silica matrix[40,41,44] and citrate anions on Au NPs. In addition, Con A with the isoelectric point in the range of 4.5−5.5[45] conjugated on the nanoprobe is also negatively charged in the neutral electrolyte solution. Thus, although the nanoprobe loaded many electroconductive Au NPs, the electrostatic repulsion between negatively charged nanoprobe and $Fe(CN)_6^{4-/3-}$ blocks the electron transfer. As seen in curve e, the binding of nanoprobes still led to a slight decrease in peak currents.

The impedance spectra are shown in Figure S1B (Supporting Information). Niquist plots comprise a semicircle part at higher frequency range and a straight linear part at lower frequency range. The diameter of the semicircle equals to the electron transfer resistance (R_{et}) at the electrode interface. Due to the good electronic transfer ability, the MWNT-modified GCE (curve b) exhibited lower R_{et} than bare GCE (curve a). It is clear that the diameter of the semicircles increased successively with sequential assembly of Con A (curve c), capture of cell (curve d), and incubation of nanoprobes (curve e), indicating an enhancement of the R_{et} step by step. These results are well consistent with the phenomena in CVs, confirming the successful preparation of the biosensor.

ECL Behavior of the Biosensor. The ECL behavior of the biosensor was investigated in 0.1 M PBS with 5 mM TPA during the CV scanning. Figure 2 shows the ECL emission as a function of potential on the biosensor. As it can be seen in curve e, the Con A@Au−$RuSiO_2$/Cell/Con A/MWNT/GCE exhibited a sensitive ECL emission starting at about 1.0 V with a peak at around 1.25 V, while the ECL intensity of Cell/Con A/MWNT/GCE (curve d) was quite low, close to the baseline.

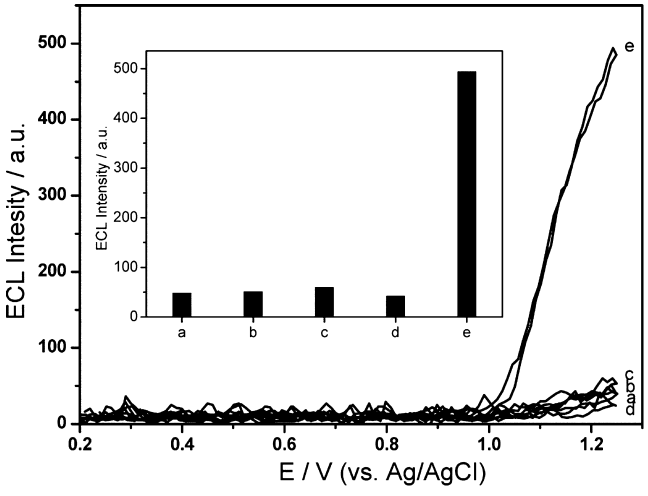

Figure 2. ECL intensity−potential curves of Con A@Au−$RuSiO_2$/MWNT/GCE (a), Con A@Au−$RuSiO_2$/Cell/MWNT/GCE (b), Con A@Au−$RuSiO_2$/Con A/MWNT/GCE (c), Cell/Con A/MWNT/GCE (d), and Con A@Au−$RuSiO_2$/Cell/Con A/MWNT/GCE (e) in 0.1 M PBS (pH 7.4) containing 5 mM TPA. CV Scan rate: 100 mV s^{-1}. The PMT voltage: 750 V. Potential: 0.2−1.25 V (vs Ag/AgCl). The concentration of K562 cells: 1.0×10^6 cells mL^{-1}. Inset: Values of the peak intensities of the corresponding ECL curves at 1.25 V.

The high ECL signal was obtained from the reaction of the doped $Ru(bpy)_3^{2+}$ with TPA, which could permeate into the silica nanoparticles through the pores of the nanoparticles. Since a single silica nanoparticle can encapsulate lots of $Ru(bpy)_3^{2+}$, it should provide large signal amplification. Meanwhile, as seen in Figure S2 (Supporting Information), the Au NPs modified at the surface of $RuSiO_2$ NPs, with excellent conductivity, can also enhance ECL response of $RuSiO_2$ NPs.

A series of control experiments was performed by the ECL measurement to verify the recognition between Con A and mannose on the cell surface and the feasibility of the biosensor. As shown in Figure 2 and the inset, all of the control electrodes presented quite weak signals. When the MWNT-modified electrode did not immobilize Con A, whenever it was followed by incubating with only nanoprobe or cell and nanoprobe, it just yielded very low ECL response (curve a and b). The reason for the phenomena is that the electrode without Con A could not capture the cells and bind the nanoprobe. In addition, when the MWNT/GCE electrode only immobilized Con A without incubation with cells, it merely brought about slight ECL emission (curve c). Moreover, without incubation of ECL nanoprobes, the electrode Cell/Con A/MWNT/GCE gave the lowest response (curve d). These results indicate that the nonspecific adsorption was very weak. Comparatively, the well-prepared biosensor under all procedures exhibited strong ECL intensity (curve e). This suggests that Con A could well recognize the mannose and trimannoside on the cell surface and capture the cells; thus, the as-proposed biosensor is sensitive and feasible.

Optimization of the Experimental Conditions. The surface density of Con A immobilized on the MWNT-modified electrode is an important parameter for capturing cells. As shown in Figure S3A (Supporting Information), a sharp increase of the ECL signal of the biosensor is observed with the increasing concentration of Con A in the solution while modifying the electrode. Then it tended to a steady value after 2.0 mg mL^{-1}, indicating a tendency for saturated surface density to thoroughly capture cells. In addition, another significant factor for capturing cells on the Con A/MWNT-coated electrode is the cell incubation time. With the increasing incubation time with 1.0×10^6 cells mL^{-1} of K562 cells, the ECL intensity of the biosensor increased and then reached a plateau at 80 min (Figure S3B, Supporting Information). Longer incubation time did not enhance the response further.

The ECL performance of the biosensor was closely related to the effect of probe incubation time and the amount of probe solution. After incubating with K562 cell suspension for 80 min, it can be seen that the ECL value increased when the nanoprobe incubation time increased, and it started to level off and slightly increase after incubation 60 min (Figure S3C, Supporting Information). Meanwhile, as shown in Figure S3D (Supporting Information), with the increasing volume of nanoprobe solution, the ECL response was significantly increased between 2.5 and 10 μL, while insignificant difference was observed for greater volumes. Therefore, the optimal conditions of biosensor were 2.0 mg mL^{-1} Con A and 80 min for cell capture and 60 min and 10 μL for nanoprobes incubation.

Cytosensing and Sensitivity of the Biosensor. On the basis of the optimal conditions, the biosensor was used for cytosensing K562 cell. Figure 3 displays the ECL signal of biosensor corresponding to K562 cell at different concen-

dx.doi.org/10.1021/ac303572g | Anal. Chem. 2013, 85, 4431−4438

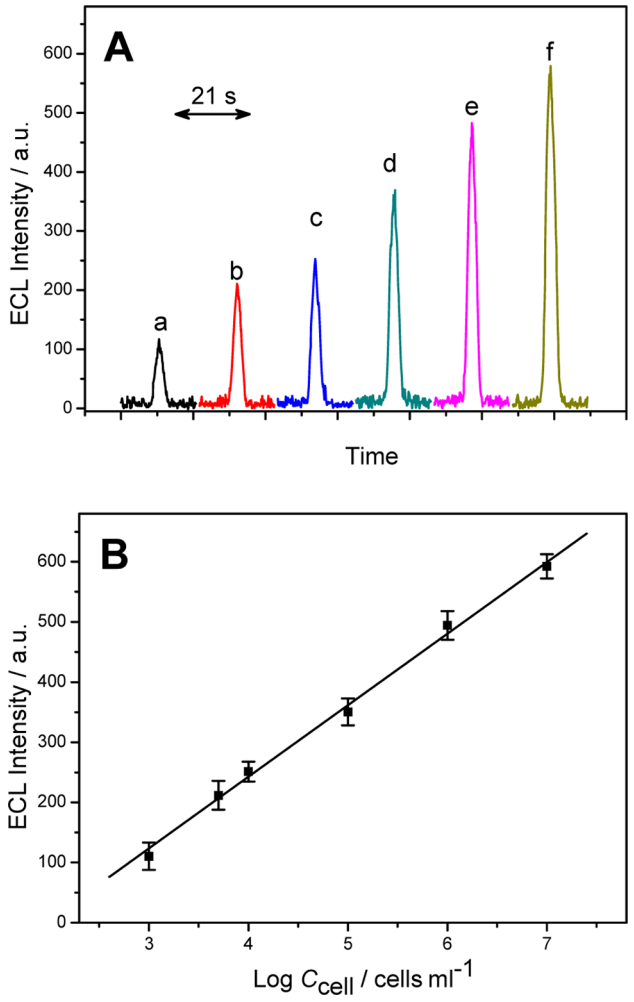

Figure 3. (A) ECL intensities versus different K562 cell concentrations (from a to f: 1.0×10^3, 5.0×10^3, 1.0×10^4, 1.0×10^5, 1.0×10^6, and 1.0×10^7 cells mL^{-1} respectively) in 0.1 M PBS (pH 7.4) containing 5 mM TPA. CV Scan rate: 100 mV s^{-1}. The PMT voltage: 750 V. Potential: 0.2−1.25 V (vs Ag/AgCl). (B) Plots of ECL intensity vs logarithm value of K562 cell concentration. The error bars were obtained from five parallel experiments.

trations. The ECL peak intensities are proportional to the logarithmic value of the cell concentration ranging from 1.0×10^3 to 1.0×10^7 cells mL^{-1}. The linear regression equation is I_{ECL} (au) = 118.9 × log C_{cell} (cells mL^{-1}) − 232.9 with the correlation coefficient of R = 0.995 (n = 5), where I_{ECL} is the ECL peak intensity and C_{cell} is the K562 cell concentration. The detection limit for cell concentration was calculated to be 600 cells mL^{-1} at 3σ. As a comparison, the electrochemical impedance technology was used to detect the K562 cell with the same procedures expect for incubation with the ECL nanoprobe. As shown in Figure S4 (Supporting Information), the detection limit using impedance was 8.1×10^3 cells mL^{-1} at 3σ. It is obvious that the sensitivity of ECL strategy is much higher than that of the impedance method. At the same time, compared to those cancer cell cytosensors using Con A as the capture or recognition element reported in the literature (Table S1, Supporting Information), the biosensor in this work displays a better performance than some earlier reported methods, especially the detection limit. It demonstrates that the proposed ECL cytosensor exhibits high sensitivity in a wide concentration range, which could be ascribed to the signal amplification of nanoprobe for the excellent immobilization of $Ru(bpy)_3^{2+}$ doped in the SiO_2 NPs and the electroactivity of Au NPs.

Stable and good ECL signals (Figure S5, Supporting Information) were obtained when the biosensor was successively scanned in 0.1 M PBS in the presence of 5 mM TPA for eight cycles. The relative standard deviation was 1.8%, signifying that the cytosensor possessed excellent potential cycling stability. The good stability of the ECL biosensor may originate from the strong electrostatic interaction between positively charged $Ru(bpy)_3^{2+}$ and negatively charged silica nanoparticles. Meanwhile, the biosensor showed the relative standard deviation of 4.8% examined for five determinations at the cell concentrations of 1.0×10^6 cells mL^{-1}, which shows the good reproducibility of the biosensor. Thus, the as-proposed biosensor exhibited good performance in detection of cancer cells with broad detection range, low detection limit, and good stability and reproducibility and is promising for monitoring carbohydrate expression of living cell.

Evaluating Cell Surface *N*-Glycan Expression under the External Stimuli of Inhibitors and Enzyme. For the cell surface, *N*-glycans have essential roles in diverse biological processes, and it remains a key pursuit to uncover their expression and myriad functions perturbed by inhibitors. The proposed biosensor was applied to evaluate the dynamic alteration of cell surface carbohydrate expression under external inhibition. Primarily, the inhibitors TM and BG were chosen to inhibit cell surface *N*-glycan and *O*-glycan expression, respectively. The expression of cell surface carbohydrate was evaluated on the basis of Con A in situ and dynamically under the inhibitory action of TM and BG for a continuous 48 h (Figure 4A). Collating the TM-treated with untreated cells, progressively decreased ECL intensity was observed. The ECL signal change was 43.6% for 48 h treatment. The decreased change of ECL response to cell surface *N*-glycan expression was caused by TM, which could block the first step in the biosynthesis of N-glycosylation in cells for inhibiting *N*-glycans.[2,46] To validate the observed change, flow cytometry is used to detect the treated K562 cells by staining with FITC-conjugated Con A. The flow cytometric value is 31.7% calculated from Figure S6 (Supporting Information), which confirmed the observed change. More importantly, the ECL strategy obtained more sensitive profiles of glycans than flow cytometry. The higher sensitivity of sensing glycans could be attributed to the sandwich architecture of biosensor and the amplification of ECL nanoprobes. Nevertheless, even though the concentration of BG (500 μM) was much higher than that of TM (1 μg mL^{-1}, approximate 1.2 μM), BG-treated cells did not show an apparent change compared to untreated cells, in both ECL and flow cytometric response. The reason is that BG could block the elaboration of the first core GalNAc residues on O-linked glycoproteins for suppressing O-glycosylation but not disturb N-glycosylation.[47,48] The distinct ECL responses of inhibition between TM and BG validate the feasibility and reliability that the majority of *N*-glycans on the cell surface could be recognized and evaluated by as-designed Con A-based glyco-biosensor.

Furthermore, enzymatic cleaving and release of *N*-glycans from asparagine was done by PNGase F, an amidase that cleaves between the innermost GlcNAc and asparagine residues of N-linked proteins.[2,49] It is noted from Figure 4B that the ECL peak intensity of PNGase F treated cells sharply dropped to 37.7% compared with untreated cells. Besides, the

dx.doi.org/10.1021/ac303572g | *Anal. Chem.* 2013, 85, 4431−4438

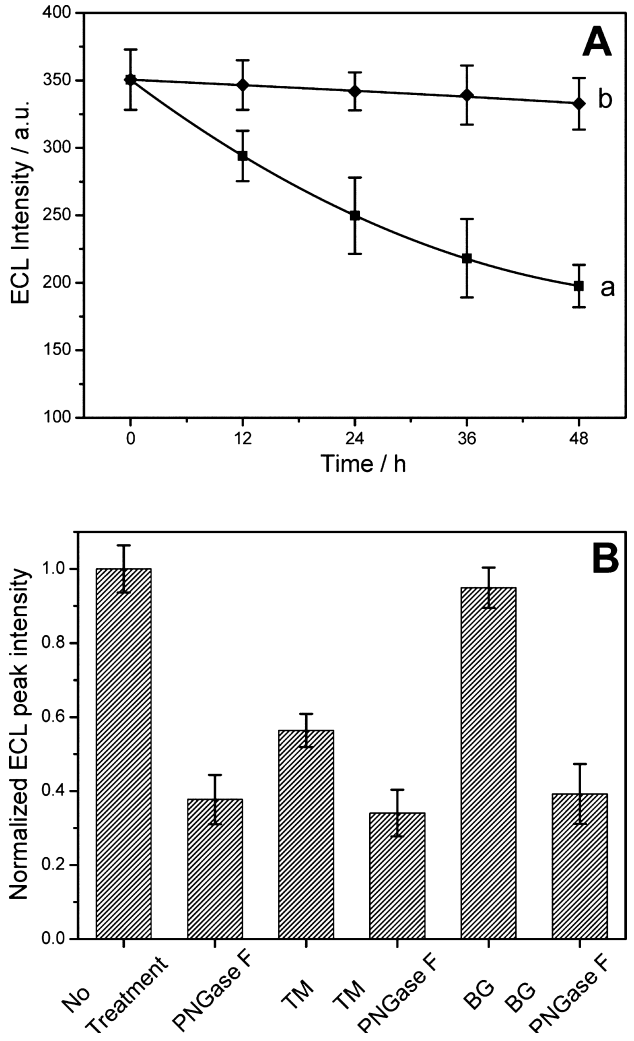

Figure 4. (A) *N*-Glycan expression of K562 cell surface treated with (a) TM (1 mg mL^{-1}) and (b) BG (500 μM) at different times. (B) *N*-Glycan expression of K562 cell surface without or with treatment of PNGase F for 24 h and after incubation with TM (1 mg mL^{-1}) and BG (500 μM) for 48 h. The ECL peak intensity was obtained at 1.25 V (vs Ag/AgCl) in 0.1 M PBS (pH 7.4) containing 5 mM TPA. CV Scan rate: 100 mV s^{-1}. The PMT voltage: 750 V. The K562 cell concentration: 1.0 × 10^5 cells mL^{-1}.

diminished result was verified by flow cytometry (Figure S7, Supporting Information), in which the mean value decreased to 44.1% after enzymatic cleaving. Whether blocked with TM, BG or not at all, the ECL signal of the biosensor was at the same level after enzymatic digesting for 24 h. Accordingly, the proposed ECL biosensor was substantiated to be able to roughly analyze *N*-glycans on cell surface. Therefore, it is indicated that the constructed biosensor not only provides a highly sensitive method for dynamically and in situ evaluating the change of cell surface *N*-glycan expression affected by inhibitors and medicine but also could be roughly applicable to screen inhibitors of *N*-glycan.

Cell Surface *N*-Glycan Expression at Different Phases of Cell Growth in Vitro. Alterations of the cell surface glycan are known to occur dynamically in response to small variation and stimuli in the extracellular and intracellular environments.[50] The ability of the biosensor to evaluate rapidly *N*-glycan enables it to be used for in situ sensing of dynamic changes in cell surface *N*-glycan during the different phases of cell growth curves in vitro. Figure 5 shows the expression of *N*-glycans on the cell surface at different times in 7 consecutive days of

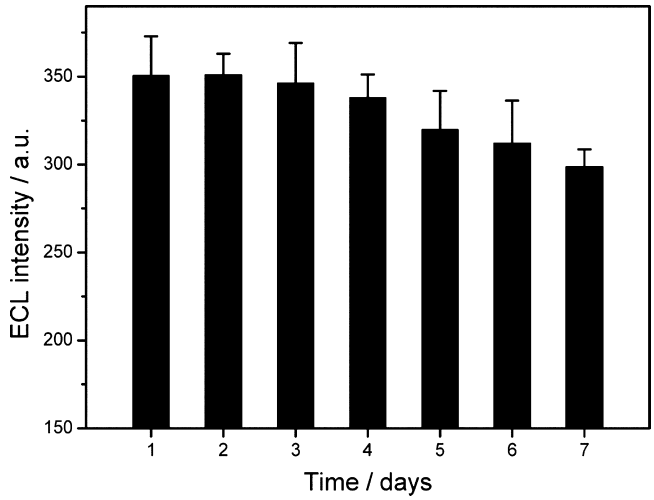

Figure 5. *N*-Glycan expression of K562 cell surface at different phases of cell growth in vitro. The ECL peak intensity was obtained at 1.25 V (vs Ag/AgCl) in 0.1 M PBS (pH 7.4) containing 5 mM TPA. CV Scan rate: 100 mV s^{-1}. The PMT voltage: 750 V. The K562 cell concentration: 1.0 × 10^5 cells mL^{-1}.

culture monitored by the as-proposed ECL biosensor. The ECL intensity was not changed before 3 days of growth, after which it appeared to decrease progressively. The decrease was confirmed by flow cytometry in Figure S8 (Supporting Information), which shows a decrease of binding to FITC–Con A after 7 days of incubation. It reveals that the cell surface *N*-glycan expression is not changed at the early stage of cell growth, while variation of *N*-glycan occurred at the later growing. When cells were in the stationary phase and later decline phase, nutrients are depleted and harmful metabolic waste products are accumulated in medium. Accordingly, the change of *N*-glycan expression on cell surface may be ascribed to the deterioration and stimulation of the medium environment. Given that the differences in *N*-glycan of glycoproteins on the cell surface are known to regulate the cell growth and arrest,[51] our results suggest that cell surface *N*-glycan plays a possible role in growth. Therefore, the biosensor has promising ability to sense in real time the changes of cell surface *N*-glycan in response to environmental stimuli and, moreover, to reveal the function of *N*-glycan in cell biology.

■ CONCLUSIONS

This work reported a novel sandwich ECL cytosensor based on the affinity of Con A recognizing and binding to mannose, especially the core trimannoside segment of *N*-glycan, for in situ and dynamically evaluating cell surface *N*-glycan expression. The distinct alteration of cell surface *N*-glycan perturbed by inhibitors TM and BG was monitored dynamically. Moreover, the variation of *N*-glycans on the cell surface at different phases of growth was also sensed in situ. The novel sandwich construction combining Con A and Au–$RuSiO_2$ NPs obtains high sensitivity and selectivity for cytosensing and evaluating most *N*-glycan expression, which is owed to the integration of advantages of bioconjuate techniques, nanotechnology, and ECL detection. This strategy provides a highly sensitive method for dynamically analyzing

dx.doi.org/10.1021/ac303572g | *Anal. Chem.* 2013, 85, 4431–4438

changes of cell surface *N*-glycan in response to inhibitors, medicines, and environmental or other stimulations. It can be expanded to provide even more impetus for elucidating the complicated mechanisms underlying *N*-glycan-related biological and physiological processes.

■ ASSOCIATED CONTENT

Supporting Information

Additional information as noted in text. This material is available free of charge via the Internet at http://pubs.acs.org.

■ AUTHOR INFORMATION

Corresponding Author

*Tel: 86-10-62795290. Fax: 86-10-62771149. E-mail: Email:jhli@mail.tsinghua.edu.cn.

Notes

The authors declare no competing financial interest.

■ ACKNOWLEDGMENTS

This work was financially supported by National Basic Research Program of China (No. 2011CB935704), the National Natural Science Foundation of China (No. 21235004, No. 21128005), and the European Union Seventh Framework Programme (FP7/2007-2013) under grant agreement No. 260600 ("GlycoHIT").

■ REFERENCES

(1) Pilobello, K. T.; Mahal, L. K. *Curr. Opin. Chem. Biol.* **2007**, *11*, 300−305.
(2) Varki, A.; Cummings, R. D.; Esko, J. D.; Freeze, H. H.; Stanley, P.; Bertozzi, C. R.; Hart, G. W.; Etzler, M. E. *Essentials of Glycobiology*, 2nd ed.; Cold Spring Harbor Laboratory Press: Plainview, NY, 2009.
(3) Dennis, J. W.; Nabi, I. R.; Demetriou, M. *Cell* **2009**, *139*, 1229−1241.
(4) Haltiwanger, R. S.; Lowe, J. B. *Annu. Rev. Biochem.* **2004**, *73*, 491−537.
(5) Gu, J. G.; Isaji, T.; Xu, Q. S.; Kariya, Y.; Gu, W.; Fukuda, T.; Du, Y. G. *Glycoconjugate J.* **2012**, *29*, 599−607.
(6) Marth, J. D.; Grewal, P. K. *Nat. Rev. Immunol.* **2008**, *8*, 874−887.
(7) Lau, K. S.; Dennis, J. W. *Glycobiology* **2008**, *18*, 750−760.
(8) Moremen, K. W.; Tiemeyer, M.; Nairn, A. V. *Nat. Rev. Mol. Cell. Biol.* **2012**, *13*, 448−462.
(9) Morishima, S.; Morita, I.; Tokushima, T.; Kawashima, H.; Miyasaka, M.; Omura, K.; Murota, S. *J. Endocrinol.* **2003**, *176*, 285−292.
(10) Marino, K.; Bones, J.; Kattla, J. J.; Rudd, P. M. *Nat. Chem. Biol.* **2010**, *6*, 713−723.
(11) Nakano, M.; Saldanha, R.; Gobel, A.; Kavallaris, M.; Packer, N. H. *Mol. Cell. Proteomics* **2011**, *10*, 1−12.
(12) Zhang, X. A.; Teng, Y. Q.; Fu, Y.; Xu, L. L.; Zhang, S. P.; He, B.; Wang, C. G.; Zhang, W. *Anal. Chem.* **2010**, *82*, 9455−9460.
(13) Royle, L.; Campbell, M. P.; Radcliffe, C. M.; White, D. M.; Harvey, D. J.; Abrahams, J. L.; Kim, Y. G.; Henry, G. W.; Shadick, N. A.; Weinblatt, M. E.; Lee, D. M.; Rudd, P. M.; Dwek, R. A. *Anal. Biochem.* **2008**, *376*, 1−12.
(14) Kaneshiro, K.; Watanabe, M.; Terasawa, K.; Uchimura, H.; Fukuyama, Y.; Iwamoto, S.; Sato, T. A.; Shimizu, K.; Tsujimoto, G.; Tanaka, K. *Anal. Chem.* **2012**, *84*, 7146−7151.
(15) Liu, X.; McNally, D. J.; Nothaft, H.; Szymanski, C. M.; Brisson, J. R.; Li, J. J. *Anal. Chem.* **2006**, *78*, 6081−6087.
(16) Naka, R.; Kamoda, S.; Ishizuka, A.; Kinoshita, M.; Kakehi, K. *J. Proteome Res.* **2006**, *5*, 88−97.
(17) Bubb, W. A. *Concepts Magn. Reson. Part A* **2003**, *19A*, 1−19.
(18) Mechref, Y.; Novotny, M. V. *Mass Spectrom. Rev.* **2009**, *28*, 207−222.
(19) Chen, S. Y.; Zheng, T.; Shortreed, M. R.; Alexander, C.; Smith, L. M. *Anal. Chem.* **2007**, *79*, 5698−5702.
(20) Shen, Z. H.; Huang, M. C.; Xiao, C. D.; Zhang, Y.; Zeng, X. Q.; Wang, P. G. *Anal. Chem.* **2007**, *79*, 2312−2319.
(21) Cheng, W.; Ding, L.; Ding, S. J.; Yin, Y. B.; Ju, H. X. *Angew. Chem., Int. Ed.* **2009**, *48*, 6465−6468.
(22) Zhang, J. J.; Cheng, F. F.; Zheng, T. T.; Zhu, J. J. *Anal. Chem.* **2010**, *82*, 3547−3555.
(23) Lis, H.; Sharon, N. *Chem. Rev.* **1998**, *98*, 637−674.
(24) Cunningham, S.; Gerlach, J. Q.; Kane, M.; Joshi, L. *Analyst* **2010**, *135*, 2471−2480.
(25) Miao, W. J. *Chem. Rev.* **2008**, *108*, 2506−2553.
(26) Xu, S. J.; Liu, Y.; Wang, T. H.; Li, J. H. *Anal. Chem.* **2011**, *83*, 3817−3823.
(27) Duan, R. X.; Zhou, X. M.; Da, X. *Anal. Chem.* **2010**, *82*, 3099−3103.
(28) Wang, Y.; Lu, J.; Tang, L. H.; Chang, H. X.; Li, J. H. *Anal. Chem.* **2009**, *81*, 9710−9715.
(29) Bertoncello, P.; Forster, R. J. *Biosens. Bioelectron.* **2009**, *24*, 3191−3200.
(30) Xu, S. J.; Liu, Y.; Wang, T. H.; Li, J. H. *Anal. Chem.* **2010**, *82*, 9566−9572.
(31) Ding, L.; Ji, Q. J.; Qian, R. C.; Cheng, W.; Ju, H. X. *Anal. Chem.* **2010**, *82*, 1292−1298.
(32) Yuan, S. R.; Yuan, R.; Chai, Y. Q.; Mao, L.; Yang, X.; Yuan, Y. L.; Niu, H. A. *Talanta* **2010**, *82*, 1468−1471.
(33) Bryce, R. A.; Hillier, I. H.; Naismith, J. H. *Biophys. J.* **2001**, *81*, 1373−1388.
(34) Debray, H.; Decout, D.; Strecker, G.; Spik, G.; Montreuil, J. *Eur. J. Biochem.* **1981**, *117*, 41−55.
(35) Dimick, S. M.; Powell, S. C.; McMahon, S. A.; Moothoo, D. N.; Naismith, J. H.; Toone, E. J. *J. Am. Chem. Soc.* **1999**, *121*, 10286−10296.
(36) Naismith, J. H.; Field, R. A. *J. Biol. Chem.* **1996**, *271*, 972−976.
(37) Macher, B. A.; Yen, T. Y. *Mol. Biosyst.* **2007**, *3*, 705−713.
(38) Bunkenborg, J.; Pilch, B. J.; Podtelejnikov, A. V.; Wisniewski, J. R. *Proteomics* **2004**, *4*, 454−465.
(39) Koles, K.; Lim, J. M.; Aoki, K.; Porterfield, M.; Tiemeyer, M.; Wells, L.; Panin, V. *Glycobiology* **2007**, *17*, 1388−1403.
(40) Qian, L.; Yang, X. R. *Adv. Funct. Mater.* **2007**, *17*, 1353−1358.
(41) Guo, Z. H.; Shen, Y.; Wang, M. K.; Zhao, F.; Dong, S. J. *Anal. Chem.* **2004**, *76*, 184−191.
(42) Innocenzi, P.; Kozuka, H.; Yoko, T. *J. Phys. Chem. B* **1997**, *101*, 2285−2291.
(43) Tai, Y.; Watanabe, M.; Murakami, J.; Tajiri, K. *J. Mater. Sci.* **2007**, *42*, 1285−1292.
(44) Zhu, Y. H.; Da, H.; Yang, X. L.; Hu, Y. *Colloids Surf., A* **2003**, *231*, 123−129.
(45) Entliche., G.; Kostir, J. V.; Kocourek, J. *Biochim. Biophys. Acta* **1971**, *236*, 795−797.
(46) Elbein, A. D. *Annu. Rev. Biochem.* **1987**, *56*, 497−534.
(47) Dube, D. H.; Prescher, J. A.; Quang, C. N.; Bertozzi, C. R. *Proc. Natl. Acad. Sci. U. S. A.* **2006**, *103*, 4819−4824.
(48) Kuan, S. F.; Byrd, J. C.; Basbaum, C.; Kim, Y. S. *J. Biol. Chem.* **1989**, *264*, 19271−19277.
(49) Tretter, V.; Altmann, F.; Marz, L. *Eur. J. Biochem.* **1991**, *199*, 647−652.
(50) Varki, A. *Cell* **2006**, *126*, 841−845.
(51) Lau, K. S.; Partridge, E. A.; Grigorian, A.; Silvescu, C. I.; Reinhold, V. N.; Demetriou, M.; Dennis, J. W. *Cell* **2007**, *129*, 123−134.